Mineralogy and Petrology (2001) 71: 31–49

Mineralogy and Petrology

Plagioclase morphologies in assimilation experiments. Implications for disequilibrium melting in the generation of granodiorite rocks

A. Castro

Department of Geology, University of Huelva, Huelva, Spain

With 5 Figures

Received December 7, 1999;
revised version accepted April 14, 2000

Summary

Assimilation experiments have been performed using a crustal contaminant and several basaltic compositions in order to study the morphologies of plagioclase crystals produced in the course of the assimilation reactions. A Crd-Bt anatectic gneiss was used as a crustal contaminant. Both a synthetic basaltic glass, with the composition of a high-Al ocean tholeiite, and a natural Hb gabbro were used as basaltic compositions. Experiments were carried out at temperatures in the range 900–1100 °C and at pressures of 4, 5 and 10 kbar. Plagioclase crystals with skeletal and honeycomb morphologies are produced in the assimilation experiments. These morphologies result from destabilisation of the crystal-melt interface caused by the disequilibrium production of a Ca-rich melt. The production of the Ca-rich metastable melt is the result of reaction between two compositionally dissimilar systems, pelite and basalt. This interpretation, based on the kinetics of plagioclase and melt production, may be applied to granodiorite rocks characterised by plagioclase with Ca-rich, skeletal cores.

Zusammenfassung

Plagioklas-Morphologie und Assimilations-Experimente: Die Bedeutung von Ungleichgewichts-Schmelzvorgängen bei der Entstehung von Granodioriten

Assimilations-Experimente mit einer krustalen Komponente und verschiedenen basaltischen Zusammensetzungen wurden durchgeführt, um die Morphologien von Plagioklas-Kristallen, die im Laufe von Assimilations-Reaktionen entstehen, zu studieren. Ein CRD-PT anatektischer Gneis wurde als krustale Beimengung benützt. Ein synthetisches basaltisches Glas mit der Zusammensetzung eines Al-reichen ozeanischen Tholeiites und ein natürlicher Hb-Gabbro wurden als basaltische Zusammensetzungen verwendet. Die Experimente wurden bei Temperaturen zwischen

900 und 1.100° und bei Drucken von 4, 5 und 10 kb durchgeführt. Plagioklas-Kristalle mit skelettartigen und Bienenwaben-förmigen Morphologien entstehen bei den Assimilations-Experimenten. Diese Morphologien sind das Ergebnis der Destabilisation der Kristall-Schmelze-Kontaktfläche, die durch die Entstehung einer im Ungleichgewicht befindlichen Ca-reichen Schmelze gefördert wird. Die Entstehung von Ca-reichen metastabilen Schmelzen geht auf die Reaktion zwischen zwei in der Zusammensetzung verschiedenen Systemen, Pelit und Basalt, zurück. Diese Interpretation, die auf der Kinetik von Plagioklas und Schmelz-Entstehung basiert, kann auf granodioritische Gesteine angewendet werden, die durch Plagioklasse mit Ca-reichen, skelettförmigen Kernen gekennzeichnet sind.

Introduction

The complex zoning patterns of plagioclase crystals found in many igneous rocks have attracted the attention of petrologists for a long time. Studies by *Vance* (1962), *Wiebe* (1968) and *Hibbard* (1981), among others, have revealed the importance of understanding plagioclase textures as a way of reconstructing magma chamber histories. Complex zoning patterns are preserved in plagioclase owing to the coupling of the $CaNa_{-1}$ interchange with the thetrahedral $AlSi_{-1}$ substitution, for which the diffusion rate (D) is very low, even at high temperature (D is about 10^{-18} cm^2s^{-1} at 1000 °C, *Grove* et al., 1984). These complex zoning patterns record complex crystal morphologies produced as the crystals grew from a silicate melt. Attempts to interpret the petrological implications of complexely zoned plagioclase crystals in igneous rocks have been made (e.g. *Hibbard*, 1981) on the basis of the end-member Ab-An system, studied by *Bowen* (1913) and *Yoder* et al. (1957). However, expriments whose aim was to produce crystal morphologies in complex silicate systems are very scarce. *Lofgren* (1974) determined experimentally the differences in morphology of plagioclase crystals produced at different rates of undercooling. The experimental studies by *Tsuchiyama* (1985a, b, c) and *Tsuchiyama* and *Takahashi* (1983) addressed the kinetics of plagioclase crystallization, melting and dissolution. Because compositional changes may be an important cause for the development of complex plagioclase zoning patterns in nature, at least in plutonic and subvolcanic environments (see *Hibbard*, 1981), we have performed experiments on mixed basalt-pelite natural systems in order to study how compositional changes control the development of complex morphologies in plagioclase crystals formed in the course of the basalt-pelite and basalt-granite reactions. The results of this experimental study are then compared to natural examples of complexely zoned plagioclase crystals from granodiorite and tonalite rocks.

Starting materials and experimental procedures

Starting materials and experimental conditions

Table 1 shows the chemical and mineralogical compositions of the starting materials used in this study. The textural and compositional features of plagioclase in the rock materials are also shown in Table 1. A synthetic high-Al olivine tholeiite (HAOT, *Patiño Douce*, 1995), and a natural Hb gabbro from Puente del Congosto near

Table 1. *Chemical and modal compositions of starting materials*

Sample	A7972	A8955	AII9648	HAOT glass
Rock type	Bt-Crd gneiss	2-mica granite	Hb gabbro	High-Al basalt
Whole-rock compositions				
SiO_2	68.6	73.4	50.09	46.9
TiO_2	0.48	0.09	0.59	0.9
Al_2O_3	15.69	14.9	12.38	18.8
FeO(t)	3.55	1.09	9.19	8.13
MnO	0.07	0.03	0.15	0.2
MgO	1.36	0.21	15.13	11.0
CaO	0.87	0.48	6.25	11.9
Na_2O	2.82	3.89	1.72	2.2
K_2O	4.56	4.47	1.41	0.1
P_2O_5	0.23	0.5	0.14	0.23
LOI	1.26	0.75	1.82	–
Total	99.93	99.94	100.01	100.00
Textural and compositional features of plagioclase				
Mol. % An	16	0 to 5	50 to 74	–
Modal abundance	12%	20%	33%	–
Zoning	No zoning	Continuous zoning	Continuous zoning	–
Morphology	Anhedral/ subhedral	Subhedral	Euhedral/ Subhedral	–

Salamanca (*Castro* et al., 1999), were used as the basalt end-members for different assimilation experiments. Experiments with the HAOT synthetic glass simulate the effect of a crystal-free melt in reaction with a pelitic gneiss. The aim of using a natural gabbro is to study the effects of pre-existing Ca-rich Pl crystals on the assimilation. Both situations are possible in nature depending on the crystal content of the basaltic magma when it intrudes and assimilates crustal rocks. The pelitic gneiss used in these assimilation experiments is a Bt-Crd anatectic gneiss (*Castro* et al., 1999). This rock was chosen because it represents a typical crustal protolith in many orogenic environments. This rock is the high-grade equivalent of the Ollo de Sapo gneiss, which is considered to be a likely crustal protolith for Iberian leucogranites (*Castro* et al., 1999, 2000). A powdered leucogranite (*Castro* et al., 1999) has also been used as a crustal contaminant, mixed in a 1:1 proportion with the HAOT synthetic glass and with 4 wt% of added water. This experiment is an attempt to reproduce a magma-mixing process in which the crustal contaminant is an anatectic granite melt rather than a migmatite. The difference is important because, (1) the activity of alumina is higher in the migmatite compared to the granite melt, and (2) in the magma-mixing case there are only reactions between melts, with no effects from pre-existing solid phases.

Experimental conditions are listed in Table 2. The characteristic assemblage produced in the assimilation experiments is Opx, Pl and a K-rich granodiorite melt, regardless of the phases present in the starting materials. Consequently, in order to

Table 2. *Experimental conditions and results of the basalt-pelite assimilation experiments*

Run N°	P (kbar)	T (°C)	Duration (h)	Vesicies	Assemblage and mode (vol. %)	Habit of plagioclase	mol.% An (in Pl)	mol.% An (in melt)
50 wt.% Hb gabbro+50 wt.% Bt, Crd gneiss								
AC19	10	1000	172	no	Opx (23), Pl (19), melt (58)	Skeletal and honeycomb	51	44
AC41	4	1000	223	yes	Opx (28), Pl (12), melt (60)	Skeletal and honeycomb	70	50
AC86	10	980 to 800	137 to 25	no	Opx (35), Pl (55), melt (10)	homeycomb, glass inclusions	50	35−25
AC95	4	900	95	yes	Opx (28), Pl (40), melt (21)	Skeletal and honeycomb	50	24
AC97	4	1100	24	yes	Opx (14), melt (77)	skeletal Opx	–	–
48 wt.% HAOT+48 wt.% Leucogranite+4 wt% added H_2O								
AC94	5	975	24	yes	Px (10), Pl (8), melt (67)	tabular, boxy	66	42
50 wt.% HAOT+50 wt% Bt, Crd gneiss								
AC99	4	980	8	no	Opx (11), Pl (42), melt (45)	Honeycomb, Opx+Pl intergrowths	62	41
AC99R	4	950	20	no	Opx (13), Pl (50), melt (41)	Honeycomb, Opx+Pl intergrowths	57	39

interpret the effects of assimilation on crystal morphologies, we need an appropriate phase diagram with the solidus and liquidus curves for our particular system Pl-Opx-melt. Some experiments have been performed in order to get the equilibrium compositions of Pl and melt at different temperatures in the range from 900 to 1100 °C and at the reference pressure of 4 kbar. Experiments at other pressures (5 and 10 kbar) were also carried out for comparison with those at 4 kbar. This pressure (4 kbar) was adopted as the reference pressure (the reference temperature is around 1000 °C) for this experimental study because based on our geological observations, it represents the most plausible conditions, at mid to upper crustal levels, at which assimilation and magma mixing occur. However, comparisons with the results at higher pressures (5 and 10 kbar) may be of interest. Finally, one temperature-programmed crystallisation experiment was conducted (Table 2, run AC 86) in order to identify possible textural changes during crystallisation.

Experimental procedure

The basaltic and crustal end-members were mechanically mixed in a weight proportion of 1:1. Such mixture is interpreted to simulate the reaction that may occur when wall rock fragments are disaggregated and assimilated in a basaltic magma chamber, or when a dense network of basaltic dikes intrudes an anatectic zone. Using powders increases the reaction kinetics so that equilibrium occurs

within 10 hours or less according to experimental tests developed for this study at temperature about 1000 °C. Experiments were carried out in end-loaded, solid-media piston-cylinder apparatus at the University of Huelva, with 12.7 mm (0.5 inch) diameter NaCl-graphite cell assemblies for experiments at pressures of 10 kbar and with CaF_2-graphite cell assemblies of the same diameter for experiments at 4 and 5 kbar. Samples were contained in welded Au capsules, 2.4 mm inner diameter with 0.3 mm wall, containing 10 mg of finely-crushed (ca. 10 μm), dry sample. In experiments with added H_2O, the appropriate amount of water was added with a microsyringe. Weight loss in capsules with added H_2O, was monitored during welding, and the capsules were also checked for leaks before the experiments by verifying that no weight loss (±0.1 mg) occurred after 2 h in an oven at 130 °C. A Pt capsule was used for an experiment at 1100 °C. Iron loss to the Pt capsule was checked by analyzing the total iron of the run product (by means of the modal abundances and mineral compositions) and comparing it with the runs using gold capsules with the same starting materials. Iron loss to the Pt capsule was less than 5 wt.% relative to Fe loss to the Au capsule. In the experiment with added water, the total duration was limited to 24 h in order to minimize water loss by diffusion through the capsule material (*Patiño Douce* and *Beard*, 1994). Capsules were examined for tears and weighed after the experiments. No weight loss was detected in the experiments reported in this paper. Temperatures were measured and controlled with Pt_{100}-$Pt_{87}Rh_{13}$ thermocouples feeding Eurotherm 808 controllers with internal ice point compensators. Temperature stability during all runs was ±5 °C. The controller was also used for programmed cooling experiments. The reported pressures are oil pressures measured with electronic DRUCK PTX 1400 pressure transmitters, feeding OMRON E5CK controllers, multiplied by ratio of ram-to-piston areas, and were manually maintained within ±5 bar of oil pressure (ca. 250 bar on the sample). Experimental products were mounted in epoxy, sawed in half and polished. Textures were studied in a SEM using backscattered electron (BSE) images (Z-contrast).

Modal compositions and EDS analyses

Modal proportions of glass (quenched melt) and neoformed phases were determined by image analysis using BSE (Z-contrast) images and the NIHimage software. The modal percentages given in Table 2 are average values from several different areas of each run. Glass and crystalline phases were analysed using a LINK-ISIS energy-dispersive spectrometer mounted on a scanning electron microscope (JEOL-JSM5410) at the University of Huelva. Operating conditions were 15 kV accelerating voltage and 100 s of effective counting time. Matrix corrections were made using the ZAF procedure. A combination of silicates, oxides and pure metals were used as standards (wollastonite for Ca and Si, jadeite for Na, orthoclase for K, corundum for Al, periclase for Mg, metallic Fe and Ti for Fe and Ti).

If the available clean surface of mineral grains or glass was large enough, the analyses were performed scanning the 1 μm beam over an area of about 6 μm^2. This technique minimises Na loss in Pl and glass, and also gives good results for the rest of the elements. Even using this procedure, Na loss from glass is appreciable, and must be corrected by measuring Na contents at 1/3 of the total counting time. We

Table 3. *Chemical compositions (in wt.%) of melts and silicate phases of the run products*

	SiO_2	TiO_2	Al_2O_3	FeO	MgO	CaO	Na_2O	K_2O	Total	100-Total	Mol % An	Habit of Pl
AC-19: 50 wt. % Hb gabbro+50 wt.% Bt, Crd gneiss (1000 °C/10 kbar)												
MELTS (n = 3)												
Average	69.26	0.86	16.68	0.88	1.08	3.35	3.02	4.87	100.00	7.65	38.0	
STD	0.45	0.08	0.15	0.49	0.18	0.19	0.07	0.13				
PLAG	56.69	0	26.96	0	0	9.53	5.03	0.88	99.09		51.1	Skeletal
	54.61	0	27.65	0	0	10.94	4.71	0.74	98.65		56.2	Skeletal
	55.06	0	27.83	0	0	11.03	4.59	0.8	99.31		57.0	Skeletal
	50.97	0	31.03	0.28	0	12.73	3.64	0.48	99.13		65.9	Rounded, relict
	51.55	0	29.52	0.43	1.21	13.08	2.83	0.6	99.22		71.9	Relict core
OPX (core)	54.35	0.32	3.32	13.24	27.56	1.08	0	0	99.87			
OPX (rim)	54.11	0.29	1.59	17.56	23.19	1.23	0	0	97.97			
AC-41: 50 wt.% Hb gabbro+50 wt.% Bt, Crd gneiss (1000 °C/4 kbar)												
MELTS (n = 6)												
Average	68.30	0.83	16.80	1.42	1.69	4.12	3.06	3.79	100.00	6.76	42.7	
STD	0.21	0.10	0.10	0.11	0.08	0.06	0.14	0.05				
PLAG	49.89	0	31.28	0	0	15.45	2.72	0.33	99.67		75.8	Skeletal
	50.74	0	30.79	0	0	14.79	2.75	0.34	99.41		74.8	Skeletal
	50.62	0	30.64	0	0	15.06	2.92	0.53	99.77		74.0	Skeletal
	51.09	0	29.25	0.67	0	13.63	2.75	0.72	98.11		73.3	Skeletal
	50.95	0.36	29.88	0.41	0	14.22	2.59	0.55	98.96		75.2	Skeletal
	52.3	0	28.84	0.43	0	13.36	3	0.69	98.62		71.1	Skeletal
	47.02	0	32.62	0	0	16.64	2.11	0.19	98.58		81.3	Rounded, relict
	47.35	0	33.16	0.36	0	16.94	1.83	0.12	99.76		83.6	Rounded, relict
OPX (core)	55.48	0.39	1.82	9.21	30.63	1.14	0	0	98.67			
OPX (rim)	54.08	0.54	1.73	16.74	25.41	1.5	0	0	100			
AC-86: 50 wt.% Hb gabbro+50 wt.% Bt, Crd gneiss (980 to 800 °C/10 kbar)												
MELTS (n = 3)												
Average	75.55	0.26	13.45	0.98	0.29	1.36	2.52	5.59	100.00	7.41	23.0	
STD	0.15	0.19	0.26	0.10	0.10	0.08	0.21	0.03				
PLAG	54.13	0	29.17	0.5	0	11.74	4.44	0.59	100.57		59.4	Skeletal
	58.39	0	25.94	0.77	0	8.69	5.1	1.43	100.32		48.5	Skeletal
	54.83	0	28.86	0.17	0	11.48	4.68	0.83	100.85		57.5	Skeletal
	54.54	0	28.54	0	0	11.46	4.25	0.96	99.75		59.8	Skeletal
AC-95: 50 wt.% Hb gabbro+50 wt.% Bt, Crd gneiss (900 °C/4 kbar)												
MELTS (n = 5)												
Average	72.64	0.31	14.28	2.18	1.07	1.25	2.61	5.65	100.00	7.48	20.9	
STD	1.45	0.16	0.96	0.34	0.51	0.54	0.21	0.39				
PLAG	47.76	0	33.19	0	0	16.36	1.86	0	99.17		82.9	Rounded, relict
	50.01	0	31.76	0.47	0	14.56	2.57	0.53	99.9		75.8	Rounded, relict
	57.11	0	26.08	0.63	0	9.37	4.68	1.25	99.12		52.5	Skeltal
	57.16	0	26.27	0.63	0	9.32	5.16	1.08	99.62		50.0	Skeltal
	58.15	0.4	24.63	0.81	0	8.25	4.13	1.93	98.3		52.5	Skeltal
OPX	54.49	0.27	1.68	16.03	25.2	1.15	0	0.15	99.32			
AC-97: 50 wt.% Hb gabbro+50 wt.% Bt, Crd gneiss (1100 °C/4 kbar)												
MELTS	60.24	0.55	16.46	3.96	2.98	4.79	3.26	3.61	95.85		44.8	
OPX	55.08	0	3.2	9.07	31.06	0.93	0	0.18	99.52			
AC-94: 48 wt% HAOT+48 wt.% Leucogranite+4 wt% water (975 °C/5 kbar)												
MELTS (n = 3)												
Average	65.12	0.62	17.73	3.79	1.67	4.83	3.30	2.95	100.00	7.82	44.7	
STD	0.34	0.08	0.14	0.11	0.07	0.08	0.27	0.08				
PLAG	56.1	0.35	25.77	1.87	0.45	10.46	3.36	1.4	99.76		63.2	Tabular
	51.8	0	30	0.58	0	13.31	3.3	0.33	99.32		69.0	Tabular
	53.82	0	27.76	0.84	0.44	11.49	3.91	0.61	98.87		61.9	Tabular
	51.59	0	29.75	0.62	0	13.37	3.41	0.32	99.06		68.4	Tabular

(*continued*)

Table 3 *(continued)*

	SiO_2	TiO_2	Al_2O_3	FeO	MgO	CaO	Na_2O	K_2O	Total	100-Total	Mol % An	Habit of Pl
OPX	54.85	0.28	7.84	12.36	20.69	2.25	0.96	0.81	100.04			
CPX	51.17	0.46	2.95	8.7	15.9	18.52	0.53	0.36	99.06			
	52.84	0.33	1.66	8.3	16.7	19.57	0.42	0	100.13			
AC-99: 50 wt.% HAOT+50 wt.% Bt, Crd gneiss (980 °C/4 kbar)												
MELTS (n = 3)												
Average	65.45	0.96	17.30	3.23	1.65	4.43	3.10	3.88	100.00	7.01	44.1	
STD	1.04	0.11	1.39	0.37	0.56	0.64	0.05	0.11				
PLAG	53.25	0	26.36	0.9	0.59	10.5	3.53	1.34	96.47		62.2	Skeletal
	53.26	0	26.8	0.94	0.44	10.86	3.82	1.21	97.33		61.1	Skeletal
	55.29	0.44	23.67	2.15	2.47	9.02	3.22	1.56	97.82		60.8	Skeletal
OPX	53.54	0.42	3.57	15.31	24.52	1.93	0	0.26	99.85			
AC-99R: 50 wt.% HAOT+50 wt.% Bt, Crd gneiss (950 °C/4 kbar)												
MELTS (n = 5)												
Average	67.72	0.97	16.11	2.91	1.48	3.02	3.29	4.50	100.00	4.43	33.6	
STD	1.54	0.14	1.64	0.61	0.45	0.85	0.44	0.31				
PLAG	54.89	0	27.36	0.58	0	10.58	4.71	0.87	98.99		55.4	Skeletal
	51.91	0.61	29.35	1.07	0.26	12.85	3.43	0.69	100.17		67.4	Skeletal
	54.95	0	27.54	0.54	0	11.15	4.89	0.68	99.75		55.8	Skeletal
	54.94	0	27.56	0.71	0	10.79	4.8	0.71	99.51		55.4	Skeletal
	54.21	0	28.47	0.66	0	11.24	4.63	0.64	99.85		57.3	Skeletal
	55.11	0	25.89	1	0.94	9.59	4.01	1.38	97.92		56.9	Skeletal
OPX	52.45	0	1.77	15.76	22.31	2.86	0	0.46	96.28			

have observed that this is the time at which the counting rate for Na starts to decrease in our hydrated glasses.

Description of the experimental products

Mineral assemblages determined in the run products are shown in Table 2. Table 3 shows the chemical compositions of melts and mineral phases (Px and Pl). No water was added to the experimental charges with the exception of the run with the leucogranite as the crustal contaminant. Approximately, 3 wt.% water is released by the hydrous minerals amphibole, biotite and cordierite in the mixed gabbro+pelitic gneiss experimental charges. Given the modal compositions, this suggests that the water content in the granitic glasses is approximately 6 wt.%. Although this water content is less than that required for saturation (e.g. *Burnham*, 1974), bubbles are present in all of the low pressure (< 6 kbar) experiments (Fig. 1). If these bubbles are interpreted as primary according to the criteria of *Dingwell* (1986), it would suggest that water saturation was reached in our experiments at a pressure of 4 kbar for a water content of approximately 6 wt.%, which is in agreement with the water solubilities in andesite melts determined experimentally by *Sakuyama* and *Kushiro* (1979).

The compositions of co-existing Pl and melt in our system are plotted in the T-X section of the Ab-An system (Fig. 2). A relevant result is that all the points at 4, 5 and 10 kbar and using different starting materials plot in a region of the T-X section of the Ab-An system very close to the region marked by the solidus and liquidus curves obtained by *Yoder* et al. (1957) and *Johannes* (1978) for the pure

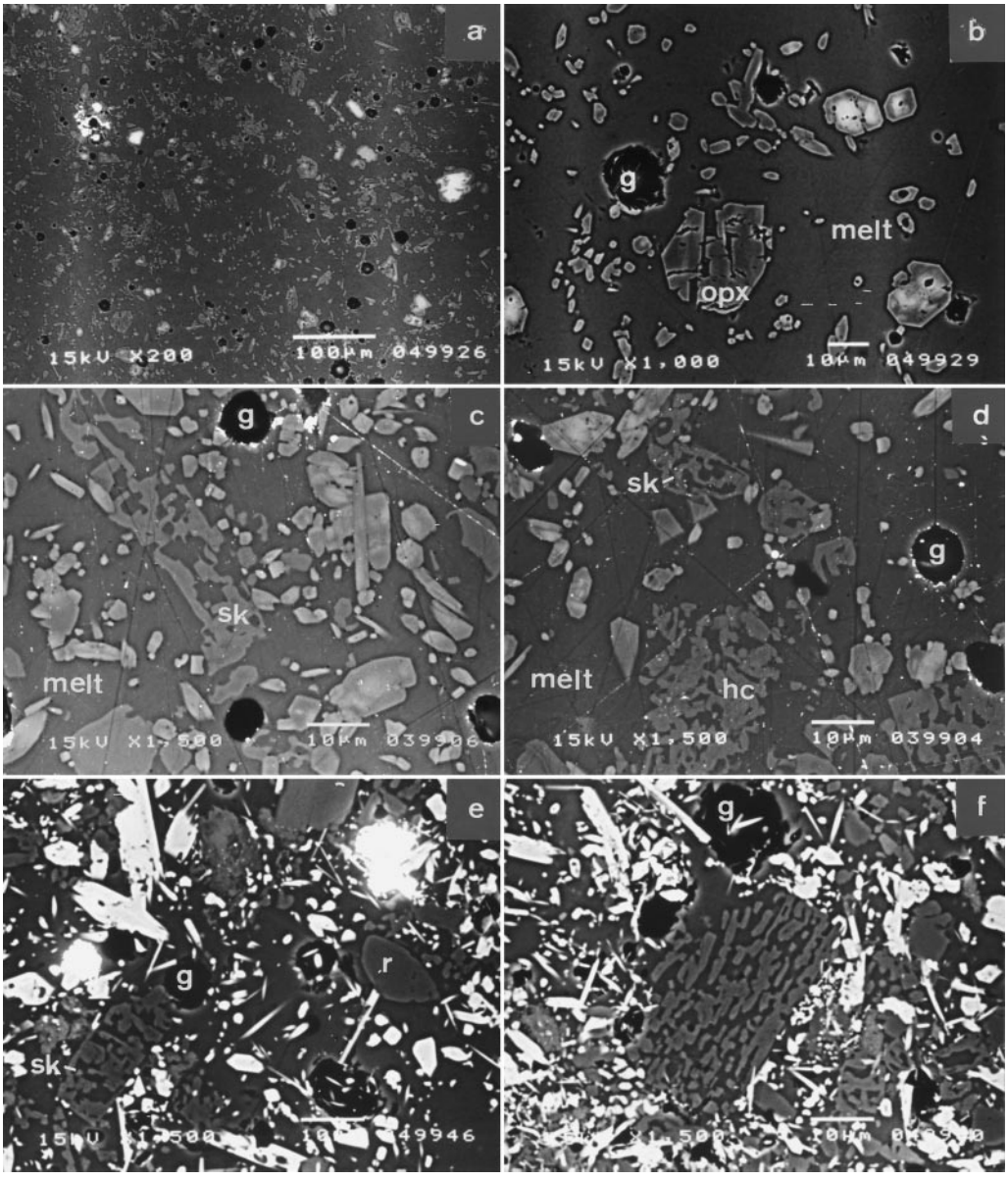

Fig. 1. Back scattered electron (BSE) images (Z contrast) of experimental runs simulating reaction of Crd-Bt anatectic gneiss with Hb gabbro. Experimental conditions and phase assembalges are summarised in Table 2. **a, b** run AC 97 (1100 °C / 4 kbar). **c, d** run AC41 (1000 °C / 4 °kbar). **e, f** run AC95 (900 °C / 4 kbar). Note the skeletal (*sk*) and honeycomb (*hc*) morphologies of Pl in experiments at 1000 and 900 °C. Black holes are primary gas bubbles (*b*); they appear in the runs at 4 kbar. Scale bar is 10 µm in **b, c, d, e, f**, and 100 µm in **a**

Ab-An system at conditions of water saturation (Fig. 2), and at temperatures of the order of 300 °C lower than those for the dry Ab-An system. It seems that the low temperatures of the solidus and liquidus curves (loop) are conditioned only by the presence of water in the system; the effect of additional phases is to modify the

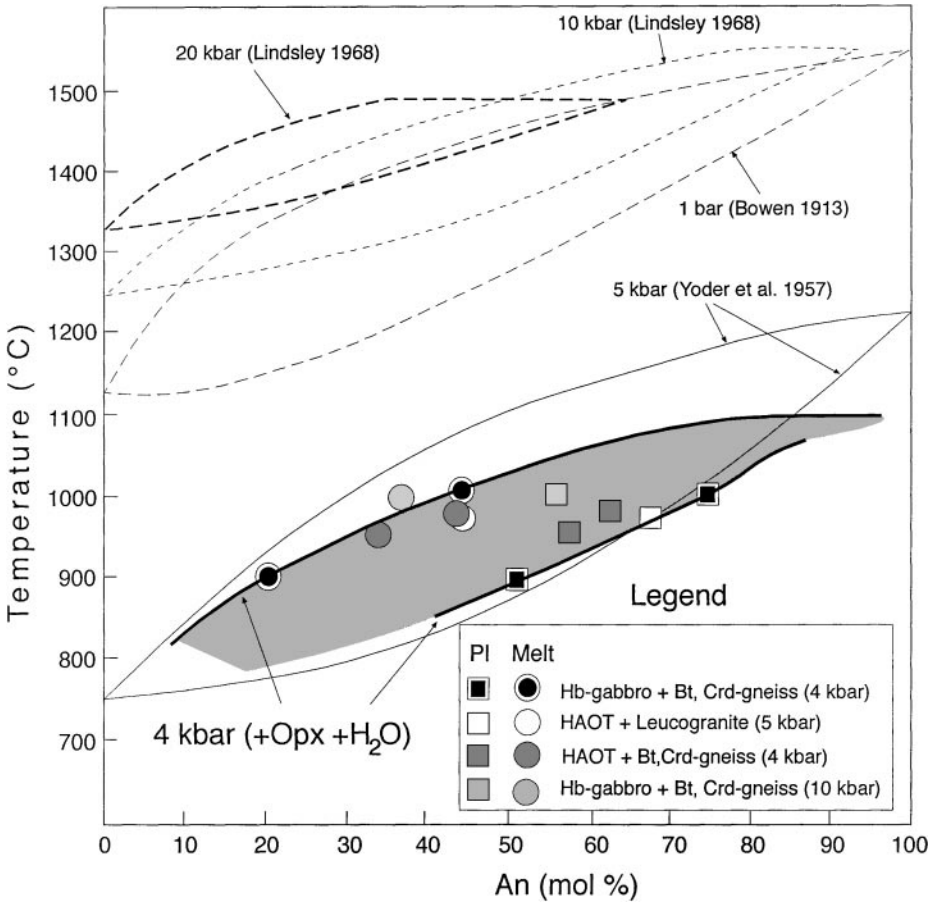

Fig. 2. T-X section of the Ab-An binary join showing the solidus and liquidus curves at different pressures and water contents. Dashed curves represent the solidus and liquidus loops for dry systems. Thin solid curves represent the loops for water saturation. The shaded area and the thick lines represent the approximate position of the loop for the natural system studied here, at a pressure of 4 kbar

slope of the loop and the width of the compositional gap between solidus and liquidus compositions (the Ca-Na partitioning coefficient). Opx in the Ab-An system reduces the slope of the curves and narrows the compositional gap compared to the loop for the pure Ab-An-water system.

Figure 1 shows BSE images of representative textures from the experiments. Plagioclases with skeletal (boxy-cellular) morphologies are present in all the experimental runs with the exception of the experiment at 1100 °C in which no Pl is present (Fig. 1a, b). In the experiments at 1000 °C both skeletal (boxy-cellular) and honeycomb (spongy-cellular, according to the nomenclature of *Hibbard*, 1995) morphologies are found (Fig. 1c, d). The composition of all the Pl crystals, with the exception of the scarce Ab-rich relicts, is homogeneous regardless of crystal morphology. This suggests that crystal/melt chemical equilibrium was reached in

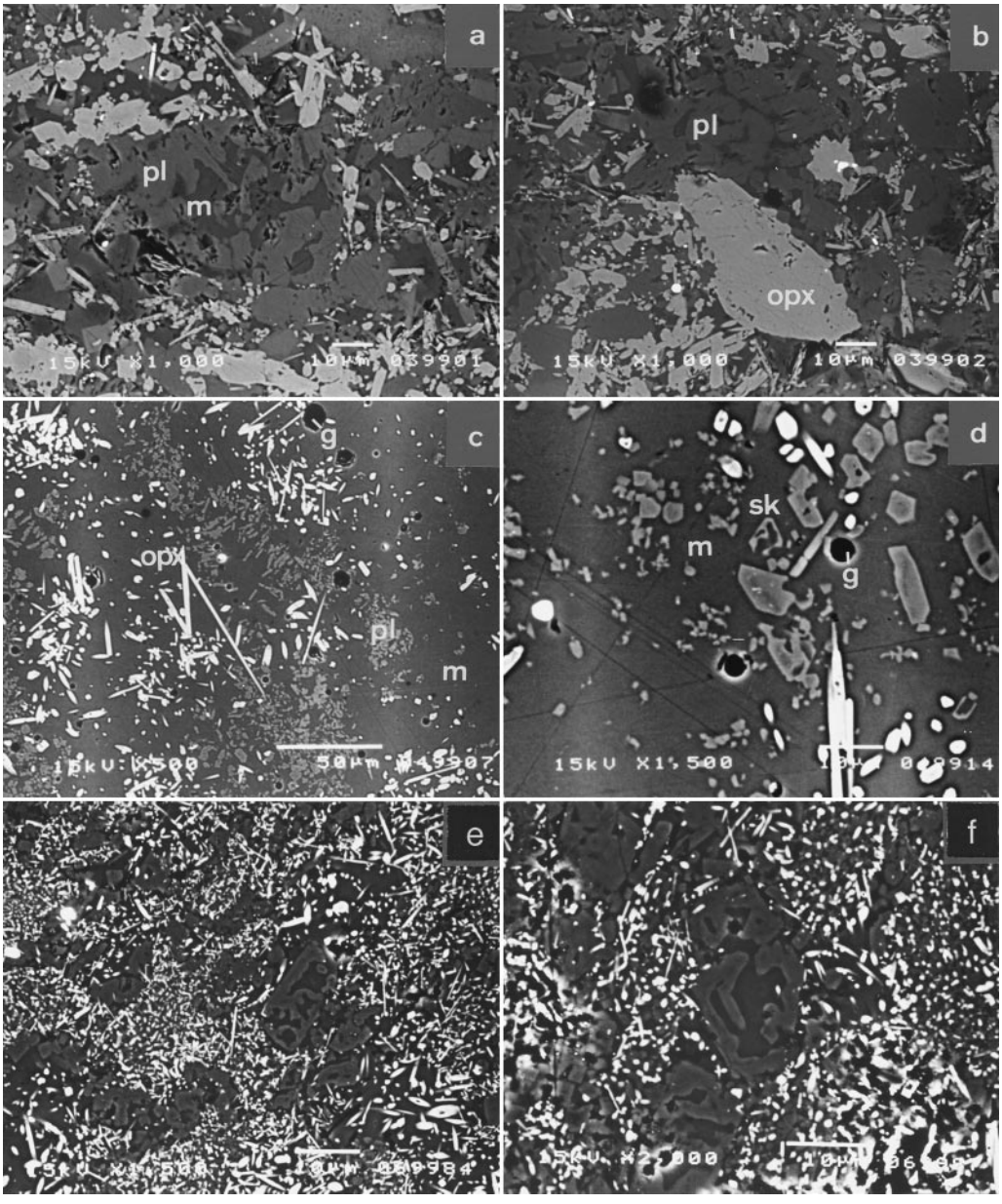

Fig. 3. **a, b** BSE (Z contrast) images of a programmed crystallisation run (AC 86). The honeycomb and skeletal morphologies produced at high temperature (980 °C) are preserved in Pl that grew outwards and inwards during slow cooling at 6 K/hour down to 800 °C. **c, d** BSE images of the run AC94 using the HAOT and a leucogranite with added water. In this run most of the neoformed plagioclase crystals have tabular morphologies. Only a few are box-shaped. **e, f** BSE images of run AC99 using the HAOT and the Crd gneiss. Scale bar is 10 µm in **a, b, d, e, f**, and 50 µm in **c**

these assimilation experiments. Skeletal crystals have euhedral faces in contact with the glass (melt) and are likely to be neoformed. Crystals with honeycomb morphologies lack regular polygonal faces and are partially dissolved. These are likely to be An-rich crystals that were present in the gabbro. The composition of these honeycomb plagioclase crystals is nearly identical to the composition of the neoformed skeletal crystals suggesting that they were re-equilibrated in the course of experiments. Ab-rich relic crystals supplied by the gneiss are very scarce. They are distinguished from those supplied by the gabbro because the Ab-rich ones have rounded outlines and preserve their original composition.

Skeletal, honeycomb and rounded crystals are found in the experiment at 900 °C (Table 2). Skeletal crystals (Fig. 1e, f) are neoformed and typically show a cellular texture in their interiors (Fig. 1f). Rounded crystals (Fig. 1e) are remnants from the Ab-rich Pl supplied by the gneiss to the mixed charge. Plagioclase compositions in the experiment at 900 °C and 4 kbar are not so homogeneous as those found in 1000 °C experiments; the composition of skeletal (neoformed) and honeycomb (partially dissolved) crystals is nearly constant around 50 mol.% Ab. The homogeneous composition of the neoformed and partially dissolved crystals indicates that diffusion in the melt allowed chemical equilibrium during melt production. The overall fractionating effect of the scarce, An-rich and Ab-rich relict cores (less than 1 vol.%) is considered negligible. In consequence, the compositions of neoformed Pl and glass from this run at 900 °C may be used to trace the position of the Ab-An loop for our particular system.

The textures resulting from the assimilation experiment with programmed cooling (Table 2) are shown in Fig. 3a and b. The compositions of Pl, Opx and glass (melt) are homogeneous. Although the melt content is very low, about 10 vol.% (Table 2), Pl crystals retain their skeletal and honeycomb morphologies which were presumably acquired during nucleation and maintained as plagioclase grew during cooling.

The textures resulting from the assimilation experiment using the synthetic HAOT and the leucogranite with added water (Table 2) are shown in Fig. 3c, d. All the Pl in this experiment is neoformed. Tabular morphologies dominate, but many skeletal and box-shaped crystals are found (Fig. 3d). Opx and Cpx are also formed in this experiment. In the experiment using the HAOT and Crd gneiss (Fig. 3e, f) all the Pl crystals have skeletal (box-shaped) morphology, similar to the textures formed in the runs using the Hb gabbro and the Crd gneiss as starting materials. The absence of Px in the starting materials for the experiment with the HAOT gives rise to a different texture for Opx, characterized by a higher nucleation density compared to the experiments using the Hb gabbro.

Discussion

In order to interpret complex zoning patterns in natural plagioclase crystals it is necessary to have knowledge of: (1) the appropriate Ab-An loop for the system's bulk composition, pressure and water content, and (2) the kinetics of plagioclase crystallization. The effects of bulk composition on the Ab-An system have been the subject of several experimental studies (see *Smith* and *Brown*, 1988 for review). Apart from bulk compositional effects, pressure and water content also affect the

position of the loop in the T-X section of the Ab-An system. Pressure has a relatively small influence on the shape and position of the Ab-An loop as demonstrated by the results of *Lindsley* (1964, 1968) at 10 and 20 kbar (Fig. 2) compared to the 1 atm loop of *Bowen* (1913) (compiled by *Morse*, 1980). The effect of pressure is strongest for Ab-rich compositions. In contrast, the effect of water on the position of the plagioclase loop, is very important as demonstrated by the water-saturated experiments of *Yoder* et al. (1957) and *Johannes* (1978) at 5 kbar. In this case the temperature of the loop is more than 300 °C lower than for dry conditions.

The Ab-An compositions of coexisting plagioclase and melt that we have determined for our particular system (Pl-Opx-granodiorite melt) provide the basis for interpreting the textures found in the experiments and also may serve as a guide for interpreting the complex zoning patterns of plagioclase crystals found in many igneous rocks.

The origin of skeletal and honeycomb plagioclase crystals

A notable result of these assimilation experiments is the formation of skeletal (box-like-cellular) and honeycomb (spongy-cellular) morphologies in plagioclase crystals (Figs. 1 and 3) at a constant temperature of 1000 °C. According to the experimental work by *Lofgren* (1964) and *Lofgren* and *Donaldson* (1975) a possible way to produce skeletal crystals is by fast (dT/dt ca. 130 K/hour) undercooling ($\Delta T = T_{\text{liquidus}} - T_{\text{equilibrium}}$) of the order of 100 °C to 200 °C. The explanation of the fact that similar kinetic effects are produced in our experiments at constant temperature, as demonstrated by the formation of skeletal crystals, lies at the heart of this discussion. Our experiments suggest that a possible mechanism to produce undercooling and skeletal plagioclase crystals is plagioclase oversaturation by assimilation of pelitic migmatites by basalt magmas. The skeletal morphologies resulting from experiments using the natural gabbro and those resulting from the experiment using the synthetic HAOT are very similar. This observation indicates that the formation of skeletal (box-like) crystals of Pl is related to the high reactivity of the mixed system resulting in a fast oversaturation in Pl. Formation of the plagioclase textures observed in the experimental products can be explained as follows (Fig. 4):

(1) Complete dissolution of Na-rich plagioclase. The Na-rich plagioclase supplied by the crustal contaminant is completely dissolved in the melt. A reaction in experiments with the Hb gabbro is the following:

$$\begin{aligned} &\text{Pl}_{(\text{gneiss})} + \text{Bt} + \text{Crd} + \text{Qtz} + \text{Al Silicate} + \text{Cpx} + \text{Hb} + \text{Pl}_{(\text{gabbro})} \\ &\quad \Rightarrow \text{Melt} + \text{Pl}_{(\text{hybrid})} + \text{Opx} \end{aligned} \tag{1}$$

Obviously, during the first stages of the experiment some metastable phases can be formed by reaction between these chemically incompatible minerals (e.g. Al Silicate and Cpx). These metastable minerals are finally consumed and/or re-equilibrated to the thermal conditions imposed in the experiments. However, the early formation of disequilibrium minerals such as Pl is recorded by its morphology (e.g. boxy cellular), which is preserved during chemical re-equilibration.

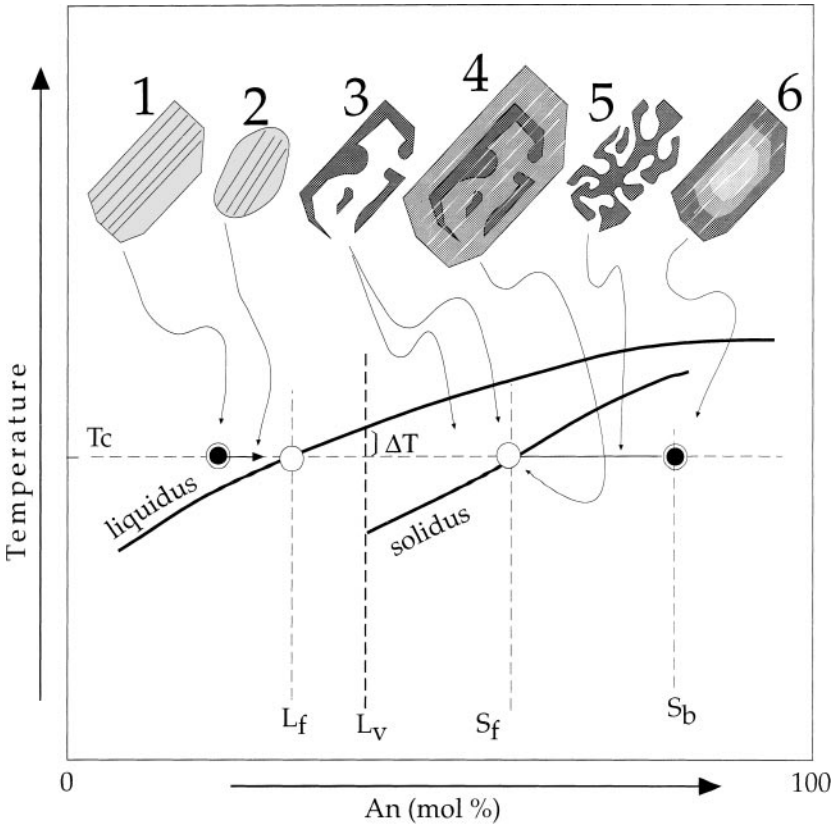

Fig. 4. Schematic diagram showing successive stages in the development of the skeletal (box-like-cellular) and honeycomb (spongy-cellular) crystals formed in the assimilation experiments. Solidus and liquidus curves are taken from Fig. 2. *Tc* is the crystallisation temperature (ca. 1000 °C in most of the assimilation experiments reported here). Zoned, Ca-rich plagioclases supplied by the Hb gabbro (*6*) are partially dissolved producing a honeycomb texture (*5*). Na-rich plagioclases supplied by the anatectic gneiss (*1*) are partially or completely dissolved (*2*). These reactions produce a non-equilibrium melt (L_v) with a composition below its liquidus. Crystals produced from this melt (*3*) will develop a skeletal (box-like-cellular) morphology, as they form at undercooling conditions (ΔT) below the liquidus. Experimental results indicate that partially dissolved Pl crystals with a Ca-rich original composition (S_b) are re-equilibrated to a final composition (S_f) in equilibrium with the final liquid (L_f) resulting from the assimilation process. Both the honeycomb (spongy-cellular) and skeletal (box-like-cellular) crystals are equilibrated at high temperatures with the final liquid (L_f) and may continue growing from this liquid giving rise to zoned crystals that preserve the skeletal cores (*4*) developed during the process of assimilation

(2) Partial dissolution of Ca-rich plagioclase. Ca-rich plagioclase supplied by the basaltic contaminant, if this a Pl-bearing magma, may have a composition outside the Ab-An loop (Fig. 4) and will thus tend to re-equilibrate its composition by dissolving in the melt producing honeycomb textures. Dissolution of Ca-rich Pl in a silicate melt was studied experimentally by *Tsuchiyama* and *Takahashi* (1983).

Their experiments produced plagioclase crystals with honeycomb textures, identical to some of the plagioclase crystals present in our assimilation experiments (Fig. 1). *Kuno* (1950) also proposed that the honeycomb plagioclase phenocrysts found in the Hakone volcano (Japan) were formed by dissolution of Ca-rich plagioclase in a silicate melt.

(3) Formation of a disequilibrium melt. The complete dissolution of the Na-rich Pl and the appearance of honeycomb textures in Ca-rich Pl crystals suggest that the processes discussed in points (1) and (2) occurred in our experiments. These processes produced a non-equilibrium melt from which a new Pl grew at the temperature of the experimental run (ca. 1000 °C). These neoformed Pl crystals have skeletal textures. The formation of skeletal morphologies is indicative of undercooling, according to the experiments of *Lofgren* (1974). In our experiments the same effect is caused by oversaturation in the Ca-rich component, which arises from the production of non-equilibrium melt. A necessary condition for this process to occur is that the formation of the metastable melt be faster than the nucleation of a new plagioclase phase. This is possible because the highly polymerised structure of Pl causes its metaestable nucleation to be more sluggish than the production of melt (*Kirpatrick*, 1983). Dissolution and melting processes are controlled by diffusion in the crystals (*Tsuchiyama* and *Takahashi*, 1983; *Tsuchiyama*, 1985a; *Lofgren* and *Norris*, 1981). Diffusion in the melt arising from local compositional gradients has a subordinate effect. Diffusion in plagioclase is controlled by the activation energy of the $NaSiCa_{-1}Al_{-1}$ exchange and the resulting diffusion coefficient (D) is of the order of $10^{-12}\,cm^2s^{-1}$ (*Tsuchiyama* and *Takahashi*, 1983). This diffusivity would allow a steady-state equilibrium between melt production and nucleation of new crystals, so that no metastable melting would occur. However, *Tsuchiyama* (1985c) obtained values of D of the order of 10^{-6} to $10^{-10}\,cm^2s^{-1}$, much larger than those predicted by the $NaSiCa_{-1}Al_{-1}$ exchange. The difference arises from the complex shape of the crystal-melt interface. If melting progresses via microfractures and cleavage planes of the crystals, then the processes of dissolution and melting are strongly favoured, yielding the apparently faster diffusion rates observed by *Tsuchiyama* (1985c).

In the case that all the CaO supplied by the basaltic magma is dissolved in the melt and no Pl crystals are present (i. e., the experiments with the HAOT synthetic glass), production of disequilibrium melt is even faster. The reaction between minerals suplied by the migmatite (e.g., Crd and Na-rich Pl) and the basaltic melt produces a melt that is oversaturated in Opx and Ca-rich Pl, causing the appearance of skeletal plagioclase crystals.

(4) Formation of skeletal plagioclase crystals. Once a non-equilibrium melt is formed in the system, it tends to crystallise rapidly because its composition lies below the liquidus curve. Crystallisation of plagioclase at small degree of undercooling is controlled by interface kinetics (*Tsuchiyama*, 1985b) rather than by diffusion in the melt. The rate of plagioclase crystallization is thus chiefly controlled by the activation energy of the $NaSiCa_{-1}Al_{-1}$ exchange. If an additional thermodynamic driving force, considerably greater than the activation energy for nucleation, is supplied by an extreme undercooling (greater than 50 °C), then the

crystal-melt interface is destabilised and the surface area of the interface increases. This process controls the shape of the crystal, which is skeletal for moderate undercooling and dendritic for extreme undercooling (*Lofgren*, 1974). It is important to note that once such a shape is acquired at the beginning of nucleation it may persist during crystal growth even after equilibrium at the crystal-melt interface is attained, as suggested by the textures found in our experiments.

Implications for the origin of granodiorite rocks

Granodiorite rocks commonly constitute large batholiths in the cores of collisional orogens as well as in active continental margins. The origin of these rocks has been controversial. On the one hand, it has been argued that they have a pure crustal origin by melting of igneous protoliths (*Chappell* and *White*, 1974; *Chappell* et al., 1987). This interpretation is based on geochemical relationships and comparisons with inferred crustal protoliths. On the other hand, a hybrid origin has been postulated involving mixing or assimilation between a crustal source component and mantle-derived basaltic melts (*Cantagrel* et al., 1984; *Reid* et al., 1983; *Collins*, 1996; *Holden* et al., 1987; *Kagami* et al., 1991; *Pankhurst* et al., 1988; *Allègre* and *Ben Othman*, 1980). The hybridisation hypothesis is supported by both isotope geochemistry and experimental studies (*Patiño Douce*, 1995; *Castro* et al., 1999). Important textural aspects, such as the complex zoning pattern in plagioclase crystals, remain controversial, in part owing to the absence of experimental studies focused on the crystallisation kinetics of these hybrid magmas.

Some examples of complex plagioclase zoning patterns found in granodiorite to tonalite rocks are shown in Fig. 5. Most of these plagioclase crystals are characterised by the presence of Ca-rich cores with varied morphologies, from skeletal (boxy-cellular) to honeycomb (spongy-cellular). One of these examples is a tonalite rock from the Adamello massif (Italian Alps). This is the Lago della Vacca tonalite, studied in detail by *Blundy* (1989) and *John* and *Blundy* (1993), and characterised by the presence of Ca-rich skeletal (box-like-cellular) cores (Fig. 5a, b) in some plagioclase crystals and Ca-rich resorbed cores (spongy-cellular) (Fig. 5c, d) in others. The compositions of the rims from both types of crystals are very similar. However, the compositions of the cores are quite different, being more anorthitic in the resorbed cores than in the skeletal ones. Resorbed cores may correspond to relict Pl supplied by the basaltic end-member and skeletal cores may have been neoformed in the course of assimilation. Another example is taken from the Quintana granodiorite (Spain) studied in detail by *Castro* (1990). This is one of the typical hybrid granodiorites formed during the Hercynian orogeny in the Iberian massif. Skeletal cores like those in Fig. 5e, f are typical of this granodiorite. The compositions of the skeletal cores and rims are very similar. The last examples (Fig. 5g, h) correspond to an Opx-bearing facies of the Quintana granodiorite. This is a subvolcanic rock and, consequently, the Pl zoning patterns are better preserved than in the plutonic facies.

The undercooling necessary to account for the observed skeletal morphologies may be caused by (cf. *Smith* and *Brown*, 1988): (1) a fast temperature drop (dT/dt ca. 130 K/hour, *Lofgren*, 1974), (2) an increase in pressure, (3) loss of water, or (4) oversaturation produced by a change in melt composition (increase in An).

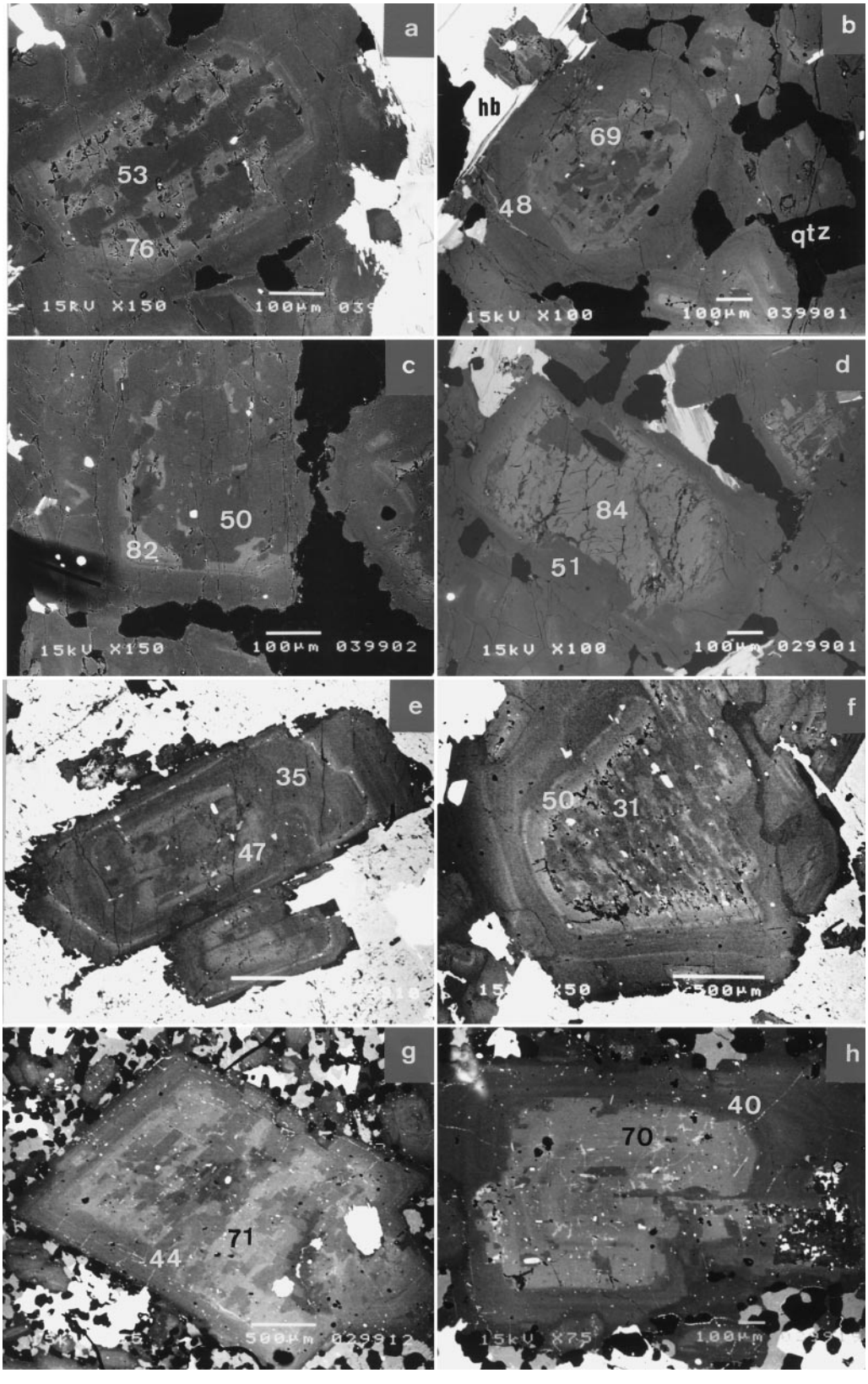
a
53
76
15kV X150
100µm
b
hb
69
48
qtz
15kV X100
100µm 039901
c
50
82
15kV X150
100µm 039902
d
84
51
15kV X100
100µm 029901
e
35
47
f
50
31
500µm
g
71
44
500µm
h
40
70
15kV X75
100µm

The first possibility is unlikely in plutonic environments because of the very fast cooling rate that is required. As regards the second possibility, an extreme increase in pressure from 1 kbar to 10 kbar produces only small changes in the plagioclase loop as discussed above. Thus, pressure or temperature changes are not likely to be the cause of skeletal plagioclase morphologies. Water loss may produce a drastic change in the position of the plagioclase loop in the T-X diagram (cf. *Hibbard*, 1995). Water loss, however, should affect all of the crystallysing phases and not just plagioclase. This is shown by dendritic textures in silicate phase (e.g. amphiboles and feldspars) that are typically found in pegmatites, and are thought to be the result of water exsolution. In granodiorites, however, skeletal textures are developed only in plagioclase crystals. Consequently, water loss may be ruled out as an effective mechanism for modifying the plagioclase phase relations in granodiorite magmas.

A mechanism that is able to produce an effective undercooling in a plutonic environment is oversaturation caused by changing the composition of the melt towards more anorthitic compositions. This process implies disequilibrium production of melt, and may be driven by either magma mixing or assimilation.

Conclusions

Skeletal and honeycomb plagioclase morphologies were produced in assimilation experiments that simulate the reaction between basaltic magmas and metamorphosed pelites in the continental crust. These plagioclase morphologies are produced by destabilisation of the crystal-melt interface due to the metastable production of a melt which is richer in Ca than the equilibrium melt. The production of a Ca-rich, non-equilibrium melt is the result of reaction between two compositionally different systems, pelite and basalt. The difference in the degree of polymerisation between melt and plagioclase is responsible for the production of metastable melt. This interpretation, which is based on the kinetics of plagioclase crystallisation as deduced from crystal morphologies, may be applied to interpret granodiorite rocks characterised by the presence of Ca-rich, skeletal cores in plagioclase.

Acknowledgements

This study is part of the project PB97-0439 funded by the Spanish Science Commission (CICYT). *H. El Hmidi* and *M. El-Biad* helped with the preparation of experimental charges. *A. Patiño Douce* provided the HAOT synthetic glass. The tonalite from the Adamello massif was collected by the author during a field trip led by *J. Blundy* and *B. John* in 1993. I also thank *C. Donaldson, M. Wolf* and an anonymous referee for their helpful comments and criticism of an earlier version of the manuscript.

Fig. 5. BSE (Z contrast) images of zoned plagioclases appearing in granodiorite and tonalite rocks of hybrid origin. **a, b** Plagioclases with skeletal (box-like-cellular) cores of the Lago della Vacca tonalite (Adamello massif, Italian Alps). **c, d** Partially dissolved, Ca-rich cores from the same tonalite. **e–h** Typical zoned plagioclase crystals from the Quintana granodiorite in the Los Pedroches batholith (Spain). Numbers refer to mol. % An. Scale bar is 100 μm in **a, b, c, d, h**; and 500 μm in **e, f, g**. Scale bar in **e** is equal to that in **f**

References

Allègre CJ, Ben Othman D (1980) Nd-Sr isotopic relationship in granitoid rocks and continental crust development: a chemical approach to orogenesis. Nature 286: 335–341

Blundy JD (1989) The geology of the southern Adamello massif, Italy. Thesis, Cambridge University

Bowen NL (1913) Melting phenomena in the plagioclase feldspars. Am J Sci 35: 577–599

Burnham CW (1974) $NaAlSi_3O_8$-H_2O solutions: a thermodynamic model for hydrous magmas. Bull Soc Mineral Crystallogr 97: 223–230

Cantagrel JM, Didier J, Gourgaud A (1984) Magma mixing: origin of intermediate rock and ''enclaves'' from volcanism to plutonism. Phys Earth Planet Interiors 35: 63–76

Castro A (1990) Microgranular enclaves of the Quintana granodiorite. Petrogenetic significance. Rev Soc Geol España 3: 7–21

Castro A, Patiño Douce AE, Corretgé LG, de la Rosa JD, El-Biad M, El-Hmidi H (1999) Origin of peraluminous granites and granodiorites, Iberian massif, Spain. An experimental test of granite petrogenesis. Contrib Mineral Petrol 135: 255–276

Castro A, Corretgé LG, El-Biad M, El-Hmidi H, Fernández C, Patiño Douce AE (2000) Experimental constraints on Hercynian anatexis in the Iberian massif, Spain. J Petrol (in press)

Chappell BW, White AJR (1974) Two contrasting granite types. Pacific Geol 8: 173–174

Chappell BW, White AJR, Wyborn D (1987) The importance of residual source material (restite) in granite petrogenesis. J Petrol 6: 1111–1138

Collins WJ (1996) Lachlan Fold Belt granitoids: products of three component mixing. Transact Roy Soc Edinburgh, Earth Sci 87: 171–181

Dingwell DB (1986) Volatile solubilities in silicate melts. In: *Scarfe CM* (ed) Short course in silicate melts. Mineralogical Association of Canada, Ottawa, pp 93–129

Grove TL, Baker MB, Kinzler RJ (1984) Coupled CaAl-NaSi diffusion in plagioclase feldspar: experiments and applications to cooling rate speedometry. Geochim Cosmochim Acta 48: 2113–2121

Hibbard MJ (1981) The magma mixing origin of mantled feldspars. Contrib Mineral Petrol 76: 158–170

Hibbard MJ (1995) Petrography to petrogenesis. Prentice Hall, Englewood Cliffs, New Jersey

Holden P, Halliday AN, Stephens WE (1987) Neodymiun and strontium isotope content of microdiorite enclaves points to mantle input to granitoid production. Nature 330: 53–56

Johannes W (1978) Melting of plagioclase in the system Ab-An-H_2O and Qz-Ab-An-H_2O at $PH_2O = 5$ kbars, an equilibrium problem. Contrib Mineral Petrol 66: 295–303

John BE, Blundy JD (1993) Emplacement related deformation of granitoid magmas, southern Adamello massif, Italy. Geol Soc Am Bull 105: 1517–1541

Kagami H, Ulmer P, Hansmann W, Dietrich V, Steiger RH (1991) Nd-Sr isotopic and geochemical characteristics of the Southern Adamello (Northern Italy) intrusives: implications for crustal versus mantle origin. J Geophys Res 96: 14331–14346

Kirkpatrick RJ (1983) Theory of nucleation in silicate melts. Am Mineral 68: 66–77

Kuno H (1950) Petrology of Hakone volcano and the adjacent areas, Japan. Bull Geol Soc Am 61: 957–1020

Lindsley DH (1964) Melting relations of plagioclase at high pressure. Carnegie Inst Washington Yearbook 63: 204–205

Lindsley DH (1968) Melting relations of plagioclase at high pressure. In: *Isachsen YW* (ed) Origin of anorthosite and related rocks. N. Y. State Museum of Science Memoir, New York, pp 479–480

Logfren G (1974) An experimental study of plagioclase crystal morphology: isothermal crystallization. Am J Sci 274: 243–273

Lofgren GE, Donaldson CH (1975) Curved branching crystals and differentiation in comb-layered rocks. Contrib Mineral Petrol 49: 309–319

Lofgren GE, Norris PN (1981) Experimental duplication of plagioclase sieve and overgrowth textures. Geol Soc Am, Abstracts with Programs, p 498

Morse SA (1984) Basalts and phase diagrams. Springer, New York

Pankhurst RJ, Hole MJ, Brook M (1988) Isotope evidence for the origin of Andean granites. Transact Roy Soc Edinburgh, Earth Sci 79: 123–133

Patiño-Douce AE (1995) Experimental generation of hybrid silicic melts by reaction of high-Al basalt with metamorphic rocks. J Geophys Res 100: 15623–15639

Patiño Douce AE, Beard JS (1994) H_2O loss from hydrous melts during fluid-absent piston-cylinder experiments. Am Mineral 79: 585–588

Reid JB, Evans OC, Fates DG (1983) Magma mixing in granitic rocks of central Sierra Nevada, California. Earth Planet Sci Lett 66: 243–261

Sakuyama M, Kushiro I (1979) Vesiculation of hydrous andesitic melt and transport of alkalis by vapor phase. Contrib Mineral Petrol 71: 61–66

Smith JV, Brown WL (1988) Feldspar minerals. Springer, Berlin Heidelberg New York

Sparks RSJ, Marshall LA (1986) Thermal and mechanical constraints on mixing between mafic and silicic magmas. J Volcanol Geotherm Res 29: 99–124

Tsuchiyama A (1985a) Partial melting kinetics of plagioclase-diopside pairs. Contrib Mineral Petrol 91: 12–23

Tsuchiyama A (1985b) Crystallization kinetics in the system $CaMgSi_2O_6$-$CaAl_2Si_2O_8$: development of zoning and kinetics effects on element partitioning. Am Mineral 70: 474–486

Tsuchiyama A (1985c) Dissolution kinetics of plagioclase in the melt of the system diopside-albite-anorthite, and origin of dusty plagioclase in andesites. Contrib Mineral Petrol 89: 1–16

Tsuchiyama A, Takahashi E (1983) Melting kinetics of plagioclase feldspar. Contrib Mineral Petrol 84: 345–354

Vance JA (1962) Zoning in igneous plagioclase: normal and oscillatory zoning. Am J Sci 260: 746–740

Wiebe R (1991) Comingling of contrasted magmas and generation of mafic enclaves in granitic rocks. In: *Didier J, Barbarin B* (eds) Enclaves and granite petrology. Elsevier, Amsterdam, pp 393–402

Wiebe RA (1968) Plagioclase stratigraphy: a record of magmatic conditions and events in a granite stock. Am J Sci 266: 690–703

Yoder HSJ, Stewart DB, Smith JR (1957) Feldspars. Carnegie Institution of Washington, Yearbook 56, pp 206–214

Author's address: *A. Castro*, Department of Geology, University of Huelva, Campus de la Rábida, E-21819 Huelva, Spain, e-mail: dorado@uhu.es